Clim Dyn
DOI 10.1007/s00382-009-0709-2

Sea ice induced changes in ocean circulation during the Eemian

Andreas Born · Kerim H. Nisancioglu · Pascale Braconnot

Received: 24 March 2009 / Accepted: 10 November 2009

Abstract We argue that Arctic sea ice played an important role during early stages of the last glacial inception. Two simulations of the Institut Pierre Simon Laplace coupled model 4 are analyzed, one for the time of maximum high latitude summer insolation during the last interglacial, the Eemian, and a second one for the subsequent summer insolation minimum, at the last glacial inception. During the inception, increased Arctic freshwater export by sea ice shuts down Labrador Sea convection and weakens overturning circulation and oceanic heat transport by 27 and 15%, respectively. A positive feedback of the Atlantic subpolar gyre enhances the initial freshening by sea ice. The reorganization of the subpolar surface circulation, however, makes the Atlantic inflow more saline and thereby maintains deep convection in the Nordic Seas. These results highlight the importance of an accurate representation of dynamic sea ice for the study of past and future climate changes.

Keywords Sea ice · Ocean circulation · Eemian · Glacial inception · Subpolar gyre · North Atlantic

A. Born (✉) · K. H. Nisancioglu
Bjerknes Centre for Climate Research,
Allegaten 55, 5007 Bergen, Norway
e-mail: andreas.born@bjerknes.uib.no

A. Born
Geophysical Institute, University of Bergen,
Allegaten 70, Bergen, Norway

P. Braconnot
IPSL/LSCE, Unité mixte CEA-CNRS-UVSQ,
Gif sur Yvette, France

1 Introduction

From paleoclimatic records, we know that warm interglacial periods, like the present Holocene (last 10,000 years) and the Eemian (129 to 113 thousand years before present), are relatively short-lived (Siegenthaler et al. 2005) and probably only stable during times of high northern latitude summer insolation. According to Milankovitch theory, an orbital configuration giving cold Northern Hemisphere summers allows snow to persist throughout the year resulting in the growth of large ice masses on land. Summer incoming shortwave radiation (insolation) at the top of the atmosphere at 65°N was at a local maximum 126,000 years before present (126 ka), followed by a minimum at 115 ka (Fig. 1) (Berger 1978). The growth of continental scale ice sheets and the transition into a full glacial, however, is generally assumed to require amplification by the internal dynamics of the climate system.

Previous model studies identified several potential feedback mechanisms amplifying the insolation signal. Retreating boreal forest over northern high latitude continents was found to lower albedo sufficiently to change local climate and favor ice growth (Calov et al. 2005; Meissner et al. 2003; de Noblet et al. 1996). Perennial snow cover is furthermore enhanced by an increased moisture convergence in the Arctic circle, result of less evaporation in a colder climate (Vettoretti and Peltier 2003). Several studies also recognize the important role of the ocean for glacial inception. Realistic snow accumulation over the Canadian Arctic is only obtained in an atmospheric model with 116 ka sea surface conditions, not present day (Yoshimori et al. 2002). Calov et al. (2005) report a subtle dependence of Scandinavian land ice growth on ocean circulation in the Nordic Seas. More intense deep

Published online: 01 December 2009

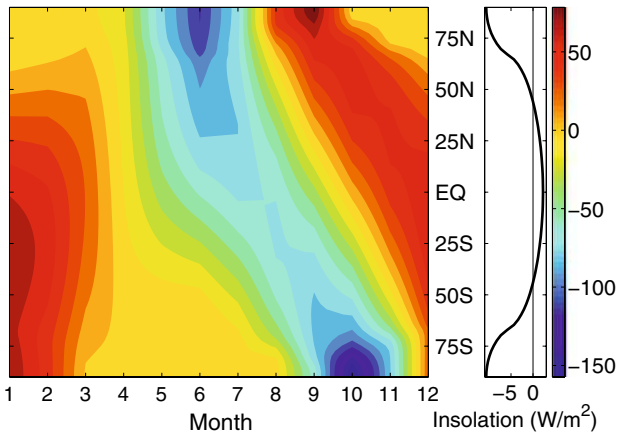

Fig. 1 Incoming short wave radiation difference at the top of the atmosphere, 115–126 ka, in W/m^2. *Left*: Seasonal variations, *right*: annual average. The seasonal cycle was reduced in high northern latitudes and the Earth received less annual mean radiation poleward of 45° at 115 ka than at 126 ka

convection results in warmer and more moist climate that increases snow accumulation.

In addition to these mechanisms, sea ice is likely to have played a major role during glacial inception. Due to its short life time, it responds quickly to changes in boundary conditions. Moreover, it provides strong feedbacks due to its high albedo in contrast to open water, its thermodynamic and mechanical decoupling of ocean and atmosphere, and due to its redistribution of freshwater in the Arctic and subarctic marine environment. Surface freshwater plays an important role for deep convection and the circulation of the deep ocean through the formation of deep water masses. A weaker deep circulation in turn implies less northward heat transport by the Atlantic meridional overturning circulation (AMOC), which can assist glacial inception. While the impact of sea ice changes on ocean circulation will be the main focus of this study, the modification of surface fluxes by sea ice also affects the growth of land ice. With more sea ice, a reduced ocean to atmosphere heat flux results in colder temperatures that favor ice growth. Concurrently, less evaporation reduces snowfall and counteracts the first process. The gross effect of a sea ice change on land ice volume thus depends on the background climate of the respective region.

Changes in the strength of deep water formation and the AMOC have often been regarded as potentially important feedback process. Gröger et al. (2007) report that in their model experiments lower sea surface temperatures result in a higher density in the North Atlantic deep water formation regions at 115 thousand years before present (115 ka) and thus a more intense AMOC than at 126 ka. Besides this direct effect of the low annual average insolation at high latitudes, the response of the ocean circulation to changes in freshwater forcing has been investigated. One such study concludes that decreased sea ice melting at 115 ka yields higher salinities in the Nordic Seas sinking regions and intensifies the AMOC compared to 126 ka (Otterå and Drange 2004). Similarly, less precipitation over the Arctic Ocean at 115 ka could have the same result (Khodri et al. 2003). On the other hand, Khodri et al. (2001) find that a weak AMOC during the last glacial inception is consistent with model results due to an increased poleward moisture transport.

A certain disagreement is evident between different models, indicating that climate interactions during the last glacial inception were highly complex and that the role of the AMOC is unclear. The present study analyzes two experiments with a state-of-the-art coupled climate model: one for the Eemian climate optimum at 126 ka and a second for the subsequent summer insolation minimum at 115 ka. The AMOC is found to be weaker at the last glacial inception (115 ka) due to enhanced advection of Arctic sea ice into the North Atlantic. The sea ice melts at the southern tip of Greenland and weakens convection in this region. Positive feedbacks due to changes in the subpolar gyre circulation enhance the freshening. These results are only expected in models explicitly including sea ice dynamics.

The climate model and the configuration of the two experiments are described in the following Sect. 2. The results are presented in Sects. 3–5, with a description of general changes in the Atlantic ocean circulation before focussing on the increase in Arctic sea ice export and the dynamic feedback related to the Atlantic subpolar gyre. The implications of the results and a discussion of the available proxy data are addressed in Sect. 6, followed by a short summary.

2 Model description and experiments

The simulations analyzed here have been carried out with the Institut Pierre Simon Laplace coupled model version 4 (IPSL CM4), comprising ocean, sea ice, atmosphere and land surface components (Marti et al. 2009). The dynamical core of the ocean model is based on the OPA system (Madec et al. 1997). The configuration used here (ORCA2) uses a horizontal resolution based on a 2 degree Mercator mesh, enhanced to 0.5 degree meridional resolution near the equator for a better representation of the equatorial wave channel and with two poles over the continents in the Northern Hemisphere in order to avoid a singularity in the Arctic Ocean. There are 31 unevenly spaced levels in the vertical. The horizontal grid resolution in northern high latitudes can be inferred from arrow spacing and the model coast line in Fig. 2. A free surface formulation is used for the upper boundary (Roullet and Madec 2000), and a diffusive boundary parametrization is used for the bottom (Beckmann 1998).

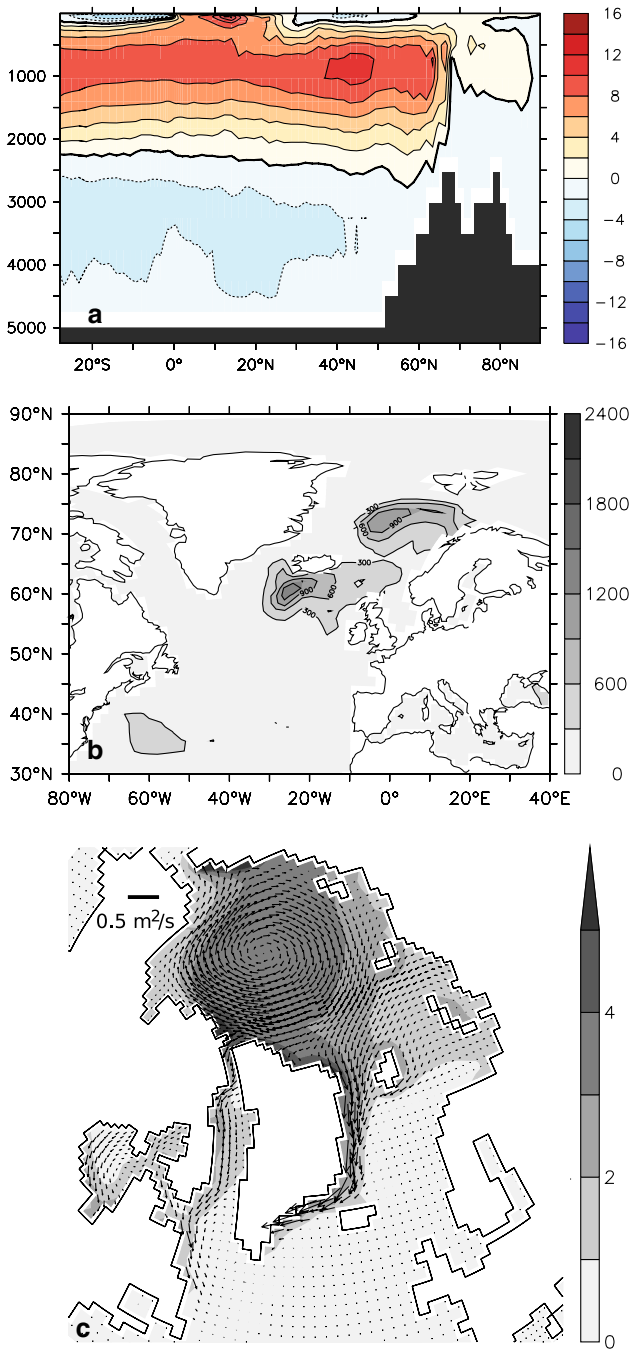

Fig. 2 Preindustrial control experiment. **a** Atlantic Meridional overturning stream function. Flow is *clockwise* around positive contour lines, in Sv. **b** Winter mixed layer depth, in m. **c** March sea ice thickness (*shading*, in m) and transport (*arrows*, scale as indicated)

The dynamic sea ice model (LIM2, Fichefet and Maqueda 1999, 1997) uses the horizontal ocean grid to compute ice rheology and advection. Thermodynamics are computed in three vertical layers, the uppermost for snow. Ice growth and melting are determined by an energy balance at both the snow-ice- and water boundary and in leads. Internal forces follow a viscous-plastic law (Hibler 1979). The model features parametrizations for the trapping of shortwave radiation by brine pockets, leads in the ice, as well as an implicit representation of subgrid variations in snow and ice thickness.

The atmosphere is simulated by a comprehensive general circulation model (LMDZ, Hourdin et al. 2006) with a resolution of 3.75 zonally and 2.5 meridionally on 19 vertical levels. Precipitation over land is returned to the ocean by means of a river routing scheme implemented in the land surface model (ORCHIDEE, Krinner et al. 2005).

This model has been used in several studies of past climate states (Braconnot et al. 2008; Zheng et al. 2008), present day climate sensitivity to anomalous freshwater forcing (Swingedouw et al. 2007b), and future projections (Swingedouw et al. 2007a; IPCC 2007).

After initializing the model with preindustrial boundary conditions, it exhibits a relatively weak AMOC of about 11 Sv (Fig. 2a). Deep convection is active in the Nordic Seas and the Irminger Basin south of Iceland (Fig. 2b). March sea ice thickness exceeds 3 m in large parts of the central Arctic Ocean (Fig. 2c). Sea ice is advected in a large anticyclonic gyre inside the Arctic Ocean and exported mainly through Fram Strait between Greenland and Spitsbergen, but also through the Canadian Archipelago and south of Spitsbergen. Although thin and not continuous, sea ice covers the entire Labrador Sea, probably preventing deep convection. The export of Arctic sea ice can only be reliably compared to modern observations by means of an area transport for which long time series exist from satellite data. A recent study estimates the maximum sea ice area export through Fram Strait between December and March to be 38,580 m^2/s (Smedsrud et al. 2008), while our preindustrial control experiment yields 46,038 m^2/s for the same time period. Overall, the model simulates thicker and more Arctic sea ice compared to present day observations, which is consistent with the lower atmospheric greenhouse gas concentration in the simulated preindustrial period. Historic records document a larger Arctic sea ice cover before the twentieth century (Divine and Dick 2006). A detailed discussion of the model's performance with present day boundary conditions and comparison with data can be found in Arzel et al. (2008).

For the present study, we analyzed two simulations forced with orbital parameters for the Eemian (126 ka) and the Last Glacial Inception (115 ka), using preindustrial greenhouse gas concentrations (Table 1) (Braconnot et al. 2008). Both experiments were initiated with an ocean at rest and preindustrial hydrography (Levitus 1982). This choice is motivated by the insufficient coverage of paleo data and relies on the assumption that the climate of the last interglacial was not fundamentally different from the present (Oppo and Lehman 1995; Müller and Kukla 2004). One potentially important difference is a significantly

Table 1 Boundary conditions for the experiments in this study. The orbital parameters were calculated following Berger (1978)

Experiment	Axial tilt (°)	Longitude of perihelion (°)	Eccentricity	CO_2 (ppm)
126 ka	23.92	112.03	0.0397	280
115 ka	22.40	291.72	0.0414	280
Preindustrial	23.46	280.84	0.0168	280

reduced height of the southern Greenland ice sheet at the last interglacial (de Vernal and Hillaire-Marcel 2008; Otto-Bliesner et al. 2006b), which is disregarded in our experiments and prescribed at its present day configuration. We believe that this simplification is not a problem for the study of the last glacial inception, which is a period of renewed ice growth.

The simulations for 126 ka and 115 ka were integrated for 300 and 800 years, respectively, and temperature drift in the lowest ocean level stabilizes at 0.06 and 0.005°C/100 years, respectively. Both sets of boundary conditions are relatively close to present day climate, and the surface ocean adjusts to the forcing in 50 years and the deep ocean in less than 150 years. The results presented are calculated from averages over the last 100 years of the simulations.

Disregarding changes in land ice, which presumably were small at the beginning of the last glacial, it is reasonable to assume that all other components of the climate system were close to equilibrium with the slowly varying insolation forcing.

3 Ocean response

Sea surface temperatures poleward of 43° latitude in the northern Pacific and Southern Ocean are lower at 115 ka, while tropical surface waters are generally warmer (Fig. 3). This can largely be attributed to a direct response to the changed orbital forcing. In the Atlantic Ocean, however, surface cooling extends further south and warming in low latitudes is more pronounced. This is the signature of a weaker oceanic heat transport Q (Fig. 4), which has been decomposed into an overturning and a horizontal component, the latter representing the large scale gyre circulation:

$$\begin{aligned} Q_{\text{total}} &= Q_{\text{overturning}} + Q_{\text{gyre}} \\ &= \rho_0 c_p \left\{ \int\int \mathrm{d}x\mathrm{d}z\overline{v}\cdot\overline{T} + \int\int \mathrm{d}x\mathrm{d}z v'\cdot T' \right\}, \end{aligned} \quad (1)$$

with reference density ρ_0, specific heat capacity of sea water c_p, the zonal averages of meridional velocity and potential temperature $(\overline{v}, \overline{T})$ and deviations thereof (v', T'). The integral spans over the entire basin width and depth (Bryden and Imawaki 2001).

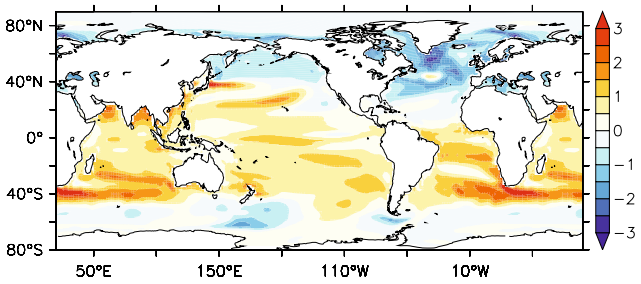

Fig. 3 Difference in annual average sea surface temperature, 115–126 ka, in °C. The zonal pattern with cold anomalies poleward of 43° latitude is a direct effect of the change in annual average insolation forcing (Fig. 1). The more southward extent of the cold anomaly in the North Atlantic, however, indicates a reorganization of the ocean dynamics

This decomposition shows that heat transport is reduced due to a reduction in overturning heat transport in most of the Atlantic, peaking at ~15°N with a reduction of 0.15 PW, or ~15%. While the overturning component increases between 40°N and 60°N, the gyre heat transport overcompensates this increase resulting in a decrease of the total heat transport. Heat transport into the Nordic Seas at 60°N is virtually unchanged. The change in Atlantic heat transport causes an asymmetric global pattern: the high latitude cooling in the Southern Hemisphere is weaker than in the Northern Hemisphere.

Consistent with the reduction in overturning heat transport, the AMOC is weaker and shallower at 115 ka with a maximum transport of 11 Sv (10^6 m^3/s) and North Atlantic Deep Water reaching down to 2,500 m depth, compared to 15 Sv and 2,900 m at 126 ka (Fig. 5). As can also be inferred from the zonally integrated stream function, the reduction in maximum transport is primarily due to a reduction in downwelling around 50°N. Waters that do not sink there carry heat further north which explains the local increase in overturning heat transport around this latitude.

Although not directly related, weaker downwelling around 50°N is accompanied by a reduction in convection in this region. At 126 ka, deep convection takes place in three different regions; the Nordic Seas, the Irminger Basin and the at the mouth of the Labrador Sea while the latter is absent at 115 ka (Fig. 6). Late winter (February and March) temperature and salinity profiles of the Labrador Sea convection region reveal that the buoyancy gain in the upper 100 m is due to freshening (Fig. 7). Below 100 m water depth, the salinity difference abates quickly while the temperature difference reverses, showing warmer subsurface waters at 115 ka, probably the result of reduced convection. The source of the surface freshening is the subject of the next section, followed by a discussion of the interaction with the gyre circulation.

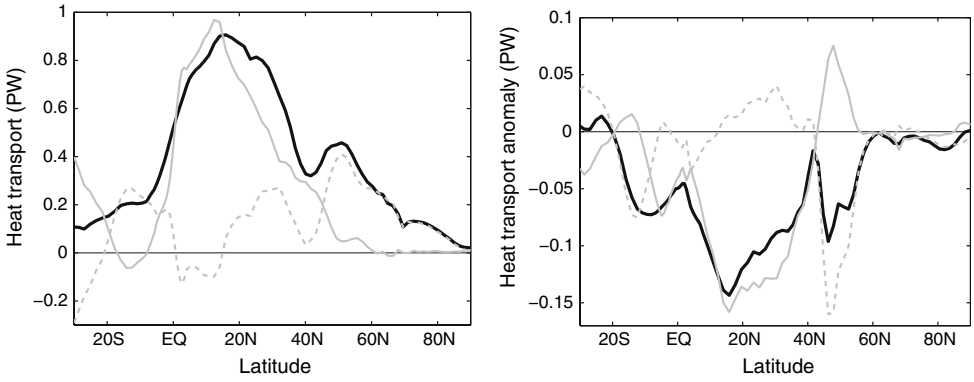

Fig. 4 Heat transport in the Atlantic Ocean (*black*), decomposed into overturning (*solid gray*) and gyre (*dashed gray*) components, *left*: 126 ka, *right*: difference 115–126 ka. The heat transport is weaker due to a weaker overturning. Around 50°N, a significantly weaker subpolar gyre reduces the heat transport

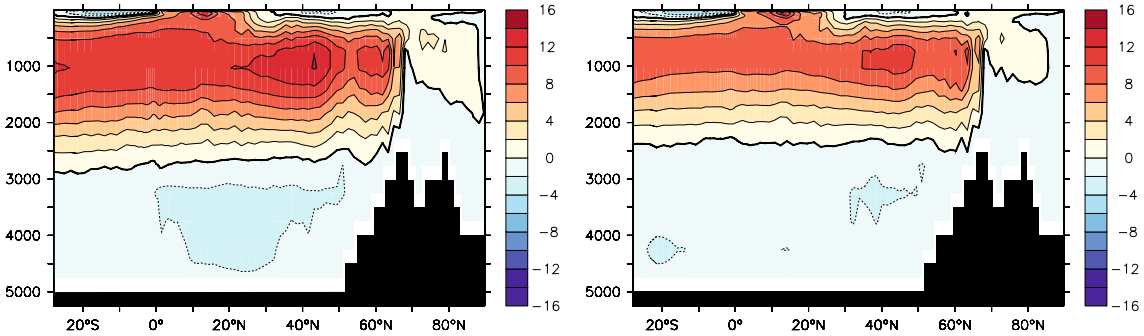

Fig. 5 Atlantic Meridional Overturning stream function. Flow is *clockwise* around positive contour lines, *left*: 126 ka, *right*: 115 ka, in Sv (10^6 m^3/s). The overturning is slightly weaker and shallower at 115 ka

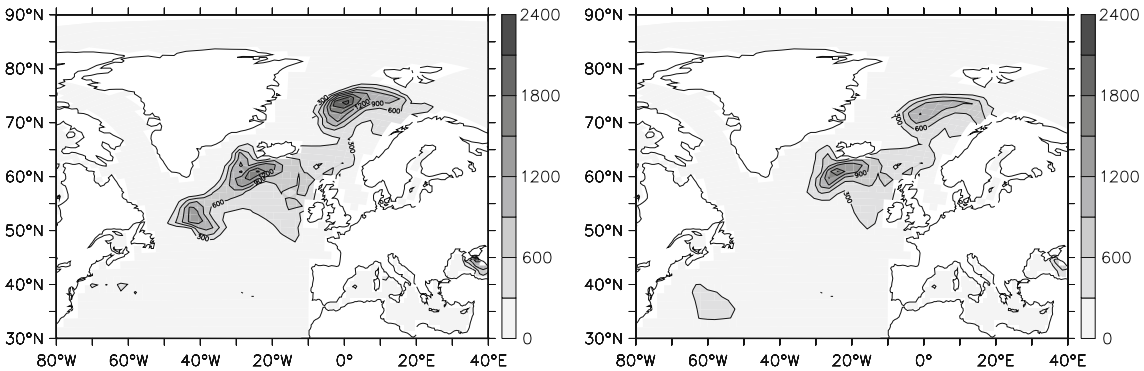

Fig. 6 Winter mixed layer depth, in m, *left*: 126 ka, *right*: 115 ka. Deep water formation occurs in three regions at 126 ka: the Nordic Seas, the Irminger Basin and off Labrador Sea. At 115 ka, Labrador Sea water formation is not active

4 Arctic sea ice export

Lower annual average insolation in high latitudes at 115 ka (Fig. 1), in particular the colder summer, gives less sea ice melting in the Arctic Ocean. Because sea ice can persist through the summer, the ice is thicker at 115 ka (Fig. 8). As a consequence, more sea ice is exported southward, almost doubling the volume transport through Fram Strait (Fig. 9). Changes in ice velocity are minor (not shown). The stronger sea ice export implies increased sea ice growth in the central Arctic which makes surface waters more saline. Thus, water exported from the Arctic in the East Greenland Current and through the Canadian Archipelago partly counteracts the freshening by sea ice. The equivalent freshwater fluxes in the upper 100 m of various sections (see Fig. 9) are calculated as follows:

$$F_t = \int_C \mathrm{d}x \int_{100\,\mathrm{m}}^{0\,\mathrm{m}} \mathrm{d}z v \frac{S - S_0}{S_0}, \tag{2}$$

where v is the northward velocity component and S the local salinity at the section. The reference salinity S_0 is taken as the average over the upper 100 m of the convection region (red box, Fig. 9) which is the depth interval of

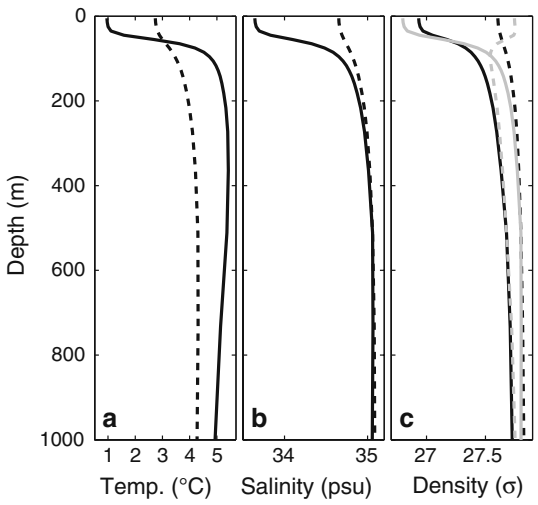

Fig. 7 Vertical profiles temporally averaged over the main convection season (February and March) and spatially over the center of the subpolar gyre (red box in Fig. 9), *solid black*: 115 ka, *dashed black*: 126 ka; *a* temperature; *b* salinity; *c* density. The *solid gray curve* in *panel c* shows the density change at 115 ka as compared to 126 ka due to salinity changes only, the *dashed gray curve* the same for temperature. Salinity changes dominate the density difference in the upper 100 m while the temperature difference plays a more important role below

most pronounced freshening (Fig. 7). In order to identify surface freshwater flux anomalies into this region, we integrate over the entire width C of the section and the upper 100 m. The zonal freshwater transport is computed likewise. Since our aim is to identify surface freshwater flux changes, sections are open at depth and the freshwater budget cannot be closed. Two sections are chosen according to the width of currents but the results do not depend critically on this choice. Freshwater transport in sea ice is based on Eq. 2 with a fixed sea ice salinity of 4 psu taken from the sea ice model. All variables are based on annual averages of the monthly model output, which itself is an average of the last 100 years of the simulations.

Only a small fraction of the Arctic freshwater export anomaly remains in the Nordic Seas. Most of the sea ice that enters the basin through Fram Strait, exits through Denmark Strait (Fig. 9). Sea ice melt produced along this pathway is largely advected through Denmark Strait by the prevailing currents. Taking into account the total freshwater transport, sea ice and liquid fraction, only 8 mSv of the total Arctic freshwater export remains in the Nordic Seas. This difference is compensated for by a stronger Atlantic inflow east of Iceland.

Ice export through Denmark Strait increases by 43 mSv at 115 ka representing a more than ninefold increase. The East Greenland Current transports 14 mSv less freshwater in 115 ka (33% less than at 126 ka) across Denmark Strait. West of Greenland, 35 mSv less freshwater is advected southward, passing through the Labrador Sea (−34%). Taken together, this results in a small salinification of the North Atlantic (−6 Sv). A decrease in evaporation and a slight increase in precipitation into the convection region yield a freshening of comparable amplitude (4 mSv, +25%).

The total freshwater transport by sea ice and ocean currents south of the Greenland Scotland Ridge is close to zero. Yet it has a strong effect on deep convection. This is due to two reasons. First, freshwater in sea ice is transported in a thin surface layer and primarily during late winter which is also the main convection season. It thus has a more concentrated effect on convection than the counteracting Arctic currents. Secondly, additional freshening is

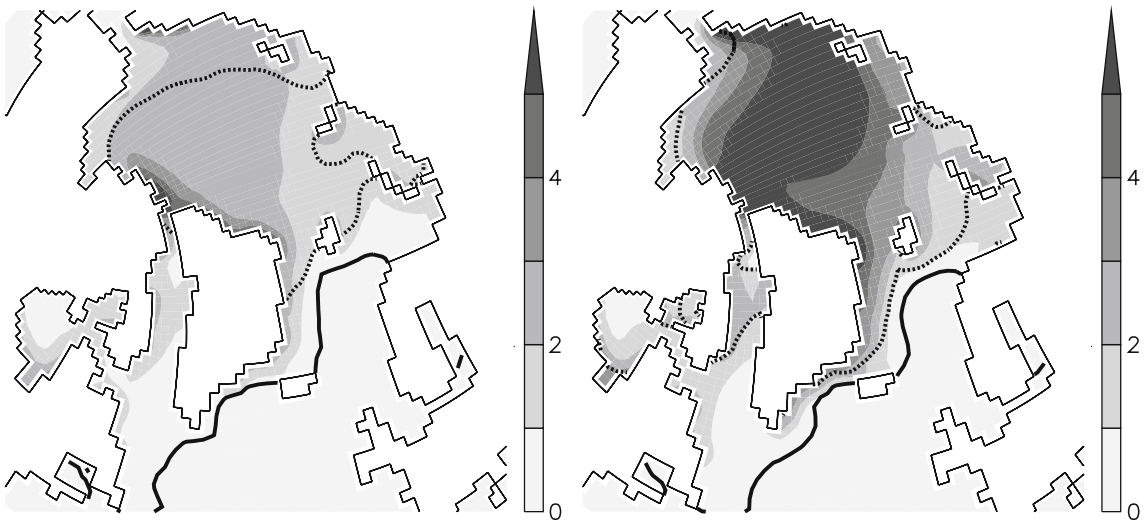

Fig. 8 Maximum winter sea ice thickness (*shading*, in m). *Lines mark* the sea ice extent defined as the area with at least 15% coverage, *solid* for winter maximum, *dashed* for summer minimum. *Left*: 126 ka, *right*: 115 ka. During summer, higher insolation melts most of the Arctic sea ice at 126 ka, resulting in thinner winter ice

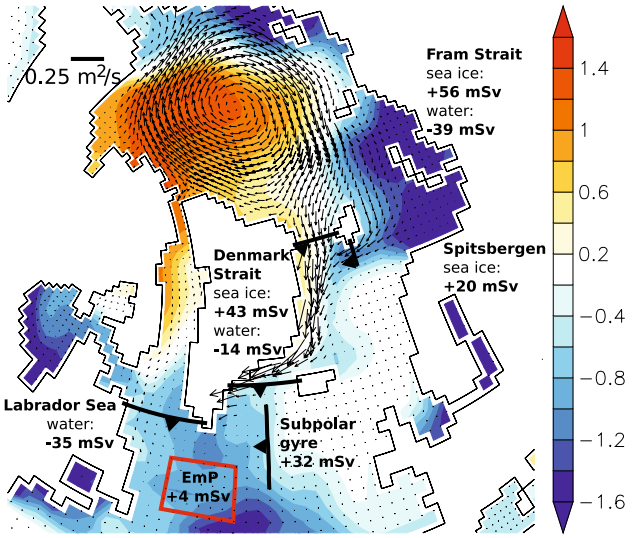

Fig. 9 Sea surface salinity (*colours*, in psu) and sea ice volume transport (*arrows*, scale as indicated) anomalies 115–126 ka. The *sections* show the corresponding freshwater transport anomalies by sea ice and ocean currents. Arctic sea ice export through Fram Strait is stronger at 115 ka, and a new path opens south of Spitsbergen. Melting of the sea ice results in fresher surface waters particularly south of Greenland. A weaker subpolar gyre advects less salt and thus contributes to the freshening of the region. *EmP*: evaporation minus precipitation

caused by a weakening of the Irminger Current. This northern branch of the subpolar gyre carries saline tropical water westward. Its weakening at 115 ka hence results in an implicit freshwater transport of 32 mSv, a fourfold increase from 126 ka.

Convection north of the Greenland Scotland Ridge is less sensitive to the increase in sea ice export. This is the result of sea ice and associated melt water in the Nordic Seas being concentrated mostly in the East Greenland Current (Fig. 9). Besides, the weaker salt transport into the western North Atlantic by the Irminger Current makes the Atlantic inflow into the Nordic Seas more saline, a mechanism that has been observed in present day climate (Hátún et al. 2005). This is seen here as an area with no salinity difference despite the general freshening trend (Fig. 9). Hence, relatively more salt is advected into the eastern Nordic Seas at 115 ka than at 126 ka, balancing the increased Arctic freshwater flux and stabilizing deep convection. Note that this reorganization of the subpolar gyre circulation and the subsequent redistribution of salt results in opposite signals for Labrador Sea and Nordic Seas convection.

5 Feedbacks of the subpolar North Atlantic

The reduction in volume transport in the Irminger Current, resulting in an implicit freshwater transport into the western North Atlantic, is a consequence of a weaker subpolar gyre, of which the Irminger Current is the northern branch. The gyre transport weakens from 26 Sv at 126 ka to 18 Sv at 115 ka (Fig. 10).

The physical reason for this circulation change is an altered density pattern in the North Atlantic. Transport changes due to wind are two orders of magnitude smaller and thus deemed negligible (Fig. 11). The subpolar gyre is at least partly controlled by the density contrast between its center and rim (Born et al. 2009; Häkkinen and Rhines 2004). A higher density in the center requires a deeper depression of the sea surface, if a level of no motion is assumed at depth where horizontal density gradients disappear. The strengthening of the gyre can thus be understood as the geostrophic response to the change in sea surface height.

To a good approximation, the changes in subpolar gyre strength seen here are the result of density changes in the upper 1,000 m in its center alone. Besides external forcing, the density in the gyre center is controlled by two positive feedbacks. The first concerns the freshening implied by a weaker gyre that reduces the density in its center and weakens the gyre even more—a positive salinity feedback (Fig. 7b). Secondly, reduced convection due to the more buoyant surface and less isopycnal diffusion as a result of

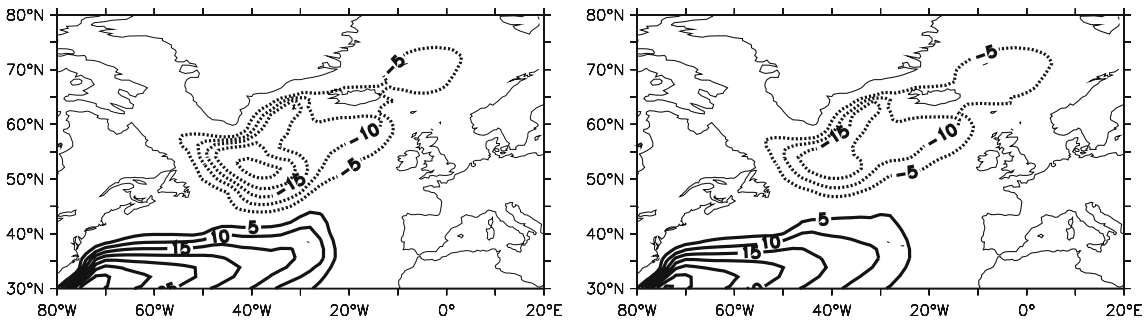

Fig. 10 Horizontal transport stream function (in Sv), negative contours denote cyclonic circulation, *left*: 126 ka, *right*: 115 ka. The subpolar gyre is approximately 30% weaker in 115 k, resulting in a weaker salt transport into the western North Atlantic by its northern branch, the Irminger Current

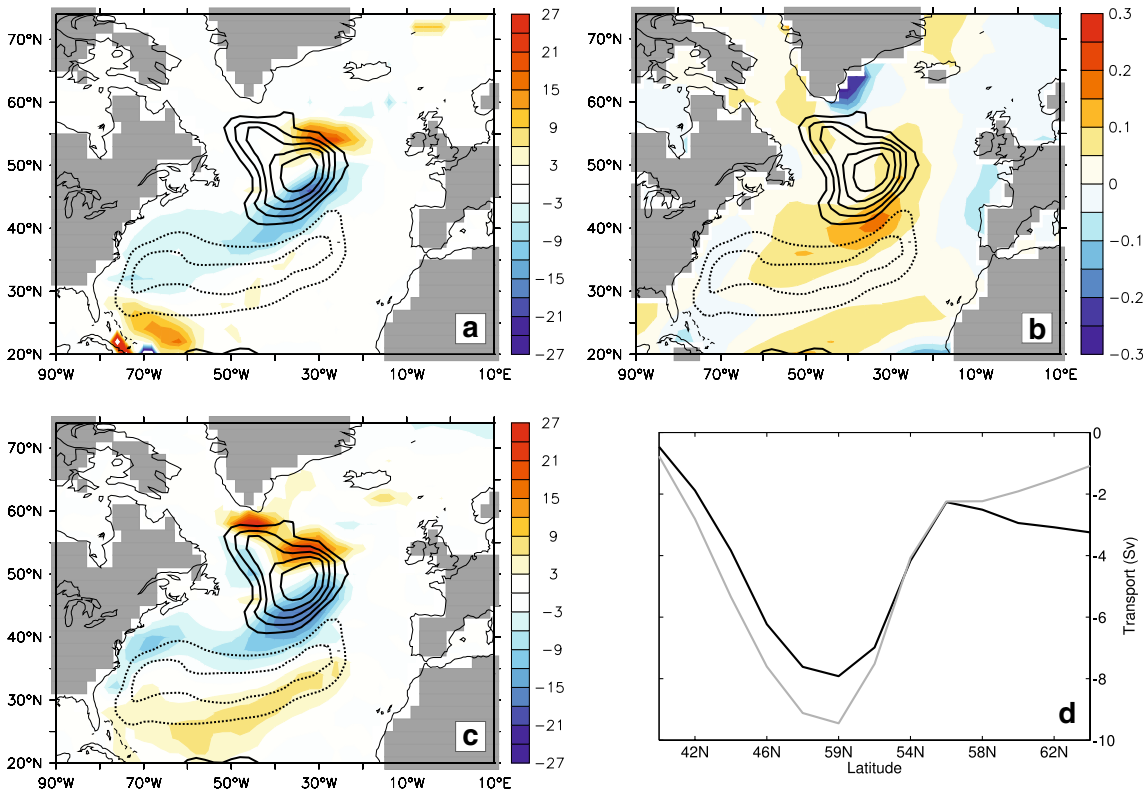

Fig. 11 Differences 115–126 ka in the vertically integrated, zonal transport are shown in *color*, *positive values* indicate eastward transport (m^2/s). Contours are the differences of the horizontal transport stream function (spacing 2 Sv) and demonstrate the spatial agreement of the changes with the subpolar gyre. The positive transport difference weakens the cyclonic subpolar gyre. **a** Vertically integrated zonal transport as computed from the density field. **b** Vertically integrated zonal transport due to changes in the wind stress. **c** Vertically integrated zonal transport as derived from the model's simulated velocities. Differences due to wind stress are small as compared to density and do not reproduce the gyre pattern. **d** Vertically integrated transport as shown in *left panels*, zonally averaged over the gyre center (40°W–20°W) and meridionally integrated in order to obtain a measure of the gyre strength difference. For details on the calculation, refer to Born et al. (2009). The *black curve* corresponds to the transport derived from the density field (**a**), the gray one to the simulated velocities (**b**). Differences in the density field generally agree with pattern and amplitude of the observed changes in the subpolar gyre

the already weaker isopycnal doming leads to a warming in subsurface waters (Fig. 7a). This again decreases the density—a positive temperature feedback (Levermann and Born 2007).

This qualitative understanding supports the interpretation that the weakening of the subpolar gyre is triggered by freshening due to Arctic sea ice export, subsequently amplified by positive feedbacks. The initial surface freshening by sea ice efficiently weakens convection in the center of the subpolar gyre. Thus, the density of the entire water column is reduced (Fig. 7c) which results in a weakening of the gyre and further freshening due to the positive feedbacks.

This allows for a better understanding of the large scale freshening in the subpolar North Atlantic. While the sea ice transport has a major impact on convection, its effect on the large scale freshening not obvious. More freshwater transported in sea ice inevitably coincides with more saline Arctic currents due to brine release. However, because sea ice triggers changes in the subpolar gyre and the associated freshwater transport, it indirectly accounts for the large scale freshening.

6 Discussion

The results presented show how changes in orbital parameters between 126 and 115 ka cause enhanced growth and export of Arctic sea ice, and how ocean circulation is reorganized in response to this redistribution of freshwater in the Arctic and subpolar North Atlantic. Most noteworthy is the shutdown of Labrador Sea Water formation and the consequent weakening of the AMOC, which has not been reported in previous studies of this time period.

Differences in complexity between climate models are the most likely reason for this discrepancy. Models previously used to simulate the last glacial inception simulated

only the thermodynamic effect of sea ice but neglected its dynamics (Khodri et al. 2001), or employed a highly simplified representation of sea ice on a zonally averaged ocean grid (Khodri et al. 2003). Both simplifications cannot accurately resolve the effect of Arctic sea ice export and the redistribution of freshwater described above. Our results also disagree with an ocean-sea ice model of higher complexity (Otterå and Drange 2004). The main difference here is that the ocean-sea ice model of this study does not simulate the atmosphere explicitly. Thus, it potentially does not capture the sensitivity of sea ice to changes in boundary conditions precisely. Moreover, the effect of changes in incoming shortwave radiation at the top of the atmosphere has to be communicated to the ocean and sea ice boundary by means of a parametrization, a source of additional uncertainties. A comparison of different models thus suggests that the representation of sea ice plays a major role in accurately simulating the last glacial inception. For lack of reliable sea ice paleo data of the last interglacial, we must assume the physically more detailed model used in the present study to capture sea ice dynamics more precisely than the examples given above.

The dynamic link between Labrador Sea convection and the subpolar gyre circulation provides a positive feedback that amplifies the surface buoyancy forcing by sea ice. A stronger gyre circulation associated with an increased density gradient between center and rim is supported by observations (Häkkinen and Rhines 2004), high resolution model studies (Spall 2004) as well as theoretical considerations (Straneo 2006).

The experiments for the present study have been carried out with present day ice sheet configuration, while observational evidence (de Vernal and Hillaire-Marcel 2008) as well as model simulations (Otto-Bliesner et al. 2006b) suggest that ice volume in southern Greenland was reduced during the Eemian. The removal of large land ice masses has two main impacts, a change in atmospheric wind patterns (Otto-Bliesner et al. 2006a) and freshwater forcing of the ocean due to increased meltwater runoff. The latter effect did probably not play a significant role during the last glacial inception since land ice masses were in a phase of regrowth. A change in wind pattern does potentially have an effect on the subpolar gyre circulation. However, we showed that changes in wind stress are negligible for our results as compared to ocean internal feedbacks (Fig. 11). The path of Arctic sea ice export in the East Greenland current is constrained by topography and hence robust to different winds.

From marine proxy data, namely dinoflagellate cysts and the oxygen isotope ratio (δ^{18}O) in foraminifera, it has been suggested that Labrador Sea convection was not active during the Eemian (Hillaire-Marcel et al. 2001). More recent data, based on the ratio of stable carbon isotopes (δ^{13}C) in foraminifera and foraminiferal assemblages, refine this view finding a convection similar to the Holocene but shifted further north in the Labrador Sea and probably starting relatively late during the last interglacial (Rasmussen et al. 2003). Silt deposits by the deep western boundary current suggest that the rate of Labrador Sea Water production was probably weaker in the Eemian than during the Holocene (Evans et al. 2007). One possible reason for a delayed onset of Labrador Sea convection is meltwater inflow from a continuously melting Greenland Ice Sheet during the early Eemian. This meltwater flux probably continued until a reorganization in deep water formation took place, dated in the Nordic Seas to approximately 125 ka (Fronval et al. 1998). Disregarding dating uncertainties in the observations, the proxy data suggests that the experiment presented for 126 ka is indeed a better analog for an ocean circulation which developed after 125 ka. This again is at least partly due to neglecting the meltwater input from a shrinking Greenland ice sheet.

Continued ventilation of the deep Atlantic and strong NADW at 115 ka finds support in several marine proxy records (Govin et al. 2009; Molyneux et al. 2007; Adkins et al. 1997). A significant reduction did probably not occur before 70 ka. However, there is evidence for a slight decrease between 126 and 115 ka (Cortijo et al. 1994; Oppo and Lehman 1995). Cortijo et al. (1994) find strong cooling and freshening in the northern Nordic Seas between 125 and 120 ka. In our simulations, this area is affected by enhanced sea ice export south of Spitsbergen. Little is known from proxy data about how the relative contributions of Nordic Seas and Labrador Sea deep waters evolved during the last glacial inception. The simulations presented here suggest that convection in the Labrador Sea is more vulnerable to changes in orbital forcing than in the Nordic Seas due to two reasons: First, sea ice is rapidly transported through the Nordic Seas in the East Greenland Current resulting in the bulk of the ice melting south of the Greenland Scotland Ridge; Secondly, a reorganization of the North Atlantic surface circulation, namely the subpolar gyre, advects less salt into the Labrador Sea and more into the Nordic Seas. The latter mechanism has previously been reported for present day climate (Hátún et al. 2005; Levermann and Born 2007).

The simulated freshening both north and south of the Greenland Scotland Ridge is relatively weak compared to present day variability (Curry and Mauritzen 2005). However, the differences presented here represent sustained changes calculated from centennial averages. Sea ice area transport decreased by almost 40% in recent years (Smedsrud et al. 2008). While incomplete data of ice thickness makes volume transport estimates difficult, the doubling of volume transport found here for the Eemian has likely not been matched in recent decades.

The Eemian interglacial has often been used as an example of a climate similar but warmer than present, and as an estimate of changes expected due to global warming by the end of this century. It must be noted that the cause of the Eemian warming was a change in insolation as compared to the future greenhouse world with a more uniform forcing over latitudes and seasons. However, model results estimate a change in sea ice export through Fram Strait of 61 mSv (Holland et al. 2006) and 70–100 mSv (Swingedouw et al. 2007a) in global warming scenarios which is comparable to the 56 mSv difference found between the Eemian and the inception. Thus, this aspect of the two different scenarios is comparable indeed although the temporal evolution is reverse. Reduced Arctic sea ice export as a result of global warming probably provides a negative feedback stabilizing Labrador Sea convection which previous studies have found to be vulnerable to warming (Vellinga and Wood 2002).

However, the stabilizing effect of reduced sea ice advection on Labrador Sea Water formation in simulations with increased levels of CO_2 is delayed with respect to local thermal buoyancy forcing. Hence, a future warming trend weakens Labrador Sea Water formation in IPSL CM4 (Swingedouw et al. 2007a) until the end of the twenty-first century, in agreement with other model studies (Holland et al. 2006; Wood et al. 1999). After this period, weaker sea ice transport balances the thermal forcing.

7 Summary

We analyzed the response of a coupled climate model to changes in insolation forcing between the last interglacial (126 ka) and the last glacial inception (115 ka). The main findings are:

- low Northern Hemisphere summer insolation allows for more sea ice growth and export of freshwater from the Arctic. More sea ice is transported south during the glacial inception than in the Eemian.
- melting of Arctic sea ice is concentrated in the Labrador Sea Water formation region and occurs mainly during late winter which is also the main convection season. It thus efficiently weakens deep water formation in the subpolar North Atlantic.
- the initial freshening by sea ice is amplified by positive feedbacks attributed to the subpolar gyre. This makes convection in the Labrador Sea more vulnerable than in the Nordic Seas.

Acknowledgments We gratefully acknowledge Oliver Marti for technical assistance as well as discussions with Tor Eldevik, Bjørg Risebrobakken, Tore Furevik and Uwe Mikolajewicz. We further thank two anonymous referees whose reviews improved our earlier manuscript. A. Born was funded by the Marie Curie Actions project NICE (MRTN-CT-2006-036127). Computer time was provided by the Centre National de la Recherche Scientifique (IDRIS computing center) and the Commissariat à l'Energie Atomique (CCRT computing center). This work is a contribution to the French ANR blanc "PICC". This is publication number A260 from the Bjerknes Centre for Climate Research.

References

Adkins JF, Boyle EA, Keigwin LD, Cortijo E (1997) Variability of the North Atlantic thermohaline circulation during the last interglacial period. Nature 390:154–156

Arzel O, Fichefet T, Goosse H, Dufresne J-L (2008) Causes and impacts of changes in the Arctic freshwater budget during the twentieth and twenty-first centuries in an AOGCM. Clim Dyn 30:37–58

Beckmann A (1998) The representation of bottom boundary layer processes in numerical ocean circulation models. In: Chassignet EP and Verron J (eds) Ocean modeling and parametrization. Kluwer, Dordrecht, pp 135–154

Berger A (1978) Long-term variations of caloric solar radiation resulting from the Earth's orbital elements. Quat Res 9:139–167

Born A, Levermann A, Mignot J (2009) Sensitivity of the Atlantic ocean circulation to a hydraulic overflow parameterisation in a coarse resolution model: response of the subpolar gyre. Ocean Model 27(3–4):130–142

Braconnot P, Marzin C, Grégoire L, Mosquet E, Marti O (2008) Monsoon response to changes in Earth's orbital parameters: comparisons between simulations of the Eemian and of the Holocene. Clim Past 4:281–294

Bryden HL, Imawaki S (2001). Ocean heat transport. In: Siedler G, Church J, Gould J (eds) Ocean circulation and climate: observing and modelling the global ocean. Acdemic Press, San Diego, pp 455–474

Calov R, Ganopolski A, Petoukhov V, Claussen M, Brovkin V, Kubatzki C (2005) Transient simulation of the last glacial inception. Part II: sensitivity and feedback analysis. Clim Dyn 24:563–576

Cortijo E, Duplessy JC, Labeyrie L, Leclaire H, Duprat J, van Weering TCE (1994) Eemian cooling in the Norwegian Sea and North Atlantic ocean preceding continental ice-sheet growth. Nature 372:446–449

Curry R, Mauritzen C (2005). Dilution of the northern North Atlantic ocean in recent decades. Science 308:1772–1774

de Noblet N, Prentice I, Joussaume S, Texier D, Botta A, Haxeltine A (1996) Possible role of atmosphere-biosphere interactions in triggering the last glaciation. Geophys Res Lett 23:3191–3194

de Vernal A, Hillaire-Marcel C (2008) Nature variability of greenland climate vegetation, and ice volume during the past million years. Science 320:1622–1625

Divine DV, Dick C (2006) Historic variability of sea ice edge position in the Nordic Seas. J Geophys Res 111:C01001

Evans HK, Hall IR, Bianchi GG, Oppo DW (2007) Intermediate water links to deep Western boundary current variability in the subtropical NW Atlantic during marine isotope stages 5 and 4. Paleoceanography 22:PA3209

Fichefet T, Maqueda MAM (1997) Sensitivity of a global sea ice model to the treatment of ice thermodynamics and dynamics. J Geophys Res 102:12609

Fichefet T, Maqueda MAM (1999) Modelling the influence of snow accumulation and snow-ice formation on the seasonal cycle of the Antarctic sea-ice cover. Clim Dyn 15:251–268

Fronval T, Jansen E, Haflidason H, Sejrup JP (1998) Variability in surface and deep water conditions in the Nordic seas during the last interglacial period. Quat Sci Rev 17:963–985

Govin A, Michel E, Labeyrie L, Waelbroeck C, Dewilde F, Jansen E (2009) Evidence for northward expansion of Antarctic Bottom Water mass in the Southern Ocean during the last glacial inception. Paleoceanography 24:PA1202. doi:10.1029/2008PA001603

Gröger M, Maier-Reimer E, Mikolajewicz U, Schurgers G, Vizcaíno M, Winguth A (2007) Changes in the hydrological cycle, ocean circulation, and carbon/nutrient cycling during the last interglacial and glacial transition. Paleoceanography 22:PA4205

Häkkinen S, Rhines PB (2004) Decline of subpolar North Atlantic circulation during the 1990s. Science 304:555–559

Hátún H, Sandø AB, Drange H, Hansen B, Valdimarsson H (2005) Influence of the atlantic subpolar gyre on the thermohaline circulation. Science 309:1841–1844

Hibler WD (1979) A dynamic thermodynamic sea ice model. J Phys Oceanogr 9:815–846

Hillaire-Marcel C, de Vernal A, Bilodeau A, Weaver AJ (2001) Absence of deep-water formation in the Labrador Sea during the last interglacial period. Nature 410:1073–1077

Holland MM, Finnis J, Serrenze MC (2006) Simulated Arctic Ocean freshwater budgets in the twentieth and twenty-first centuries. J Clim 19:6221–6242

Hourdin F, Musat I, Bony S, Braconnot P, Codron F, Dufresne J, Fairhead L, Filiberti M, Friedlingstein P, Grandpeix J, Krinner G, Levan P, Li Z, Lott F (2006) The LMDZ4 general circulation model: climate performance and sensitivity to parametrized physics with emphasis on tropical convection. Clim Dyn 27(7–8):787–813

IPCC (2007) Climate Change 2007: The Physical Science Basis. In: Solomon S, Qin D, Manning M, Chen Z, Marquis M, Averyt KB, Tignor M, Miller HL (eds) Contribution of Working Group I to the fourth assessment report of the intergovernmental panel on climate change. Cambridge University Press, Cambridge

Khodri M, Leclainche Y, Ramstein G, Braconnot P, Marti O, Cortijo E (2001) Simulating the amplification of orbital forcing by ocean feedbacks in the last glaciation. Nature 410:570–574

Khodri M, Ramstein G, Paillard D, Duplessy C, Kageyama M, Ganopolski A (2003) Modelling the climate evolution from the last interglacial to the start of the last glaciation: the role of arctic ocean freshwater budget. Geophys Res Lett 30(12):1606

Krinner G, Viovy N, de Noblet-Ducoudre N, Ogee J, Polcher J, Friedlingstein P, Ciais P, Sitch S, Prentice IC (2005) A dynamic global vegetation model for studies of the coupled atmosphere–biosphere system. Glob Biogeochem Cycles 19(1):GB1015

Levermann A, Born A (2007) Bistability of the Atlantic subpolar gyre in a coarse-resolution model. Geophys Res Lett 34:L24605

Levitus S (1982) Climatological atlas of the world ocean. NOAA Professional Paper, vol 13. US Department of Commerce, Washington, DC

Madec G, Delecluse P, Imbard M, Lévy C (1997) OPA version 8.1 Ocean General Circulation Model reference manual. Institut Pierre-Simon Laplace, Note du Pôle de modélisation no. 11

Marti O, Braconnot P, Dufresne J-L, Bellier J, Benshila R, Bony S, Brockmann P, Cadule P, Caubel A, Codron F, de Noblet N, Denvil S, Fairhead L, Fichefet T, Foujols M-A, Friedlingstein P, Goosse H, Grandpeix J-Y, Guilyardi E, Hourdin F, Idelkadi A, Kageyama M, Krinner G, Lévy C, Madec G, Mignot J, Musat I, Swingedouw D, Talandier C (2009) Key features of the IPSL ocean atmosphere model and its sensitivity to atmospheric resolution. Clim Dyn 34(1):1–26. doi:10.1007/s00382-009-0640-6

Meissner KJ, Weaver AJ, Matthews HD, Cox PM (2003) The role of land surface dynamics in glacial inception: a study with the UVic Earth system model. Clim Dyn 21:515–537

Molyneux EG, Hall IR, Zahn R, Diz P (2007) Deep water variability on the southern Agulhas Plateau: interhemispheric links over the past 170 ka. Paleoceanography 22:PA4209

Müller UC, Kukla GJ (2004) North Atlantic Current and European environments during the declining stage of the last interglacial. Geology 32:1009–1012

Oppo DW, Lehman SJ (1995) Suborbital timescale variability of North Atlantic deep water during the past 200,000 years. Paleoceanography 10(5):901–910

Otterå OH, Drange H (2004). Effects of solar irradiance forcing on the ocean circulation and sea-ice in the North Atlantic in an isopycnic coordinate ocean general circulation model. Tellus 56A:154–166

Otto-Bliesner BL, Brady E, Clauzet G, Tomas R, Levis S, Kothavala Z (2006a) Last glacial maximum and holocene climate in CCSM3. J Clim 19:2526–2544

Otto-Bliesner BL, Marshall SJ, Overpeck JT, Miller GH, Hu A, CAPE Last Interglacial Project members (2006b) Simulating arctic climate warmth and icefield retreat in the last interglaciation. Science 311:1751–1753

Rasmussen TL, Oppo DW, Lehman ETSJ (2003). Deep sea records from the southeast Labrador Sea: ocean circulation changes and ice-rafting events during the last 160,000 years. Paleoceanography 18(1):1018

Roullet G, Madec G (2000). Salt conservation, free surface, and varying levels: a new formulation for ocean general circulation models. J Geophys Res 105:23927–23942

Siegenthaler U, Stocker TF, Monnin E, Lüthi D, Schwander J, Stauffer B, Raynaud D, Barnola J-M, Fischer H, Masson-Delmotte V, Jouzel J (2005) Stable carbon cycle-climate relationship during the late Pleistocene. Science 310:1313–1317

Smedsrud LH, Sorteberg A, Kloster K (2008) Recent and future changes of the arctic sea-ice cover. Geophys Res Lett 35:L20503

Spall MA (2004) Boundary currents and watermass transformation in marginal seas. J Phys Oceanogr 34:1197–1213

Straneo F (2006) On the connection between dense water formation, overturning, and poleward heat transport in a convective basin. J Phys Oceanogr 36:1822–1840

Swingedouw D, Braconnot P, Delecluse P, Guilyardi E, Marti O (2007a) Quantifying the AMOC feedbacks during a 2 × CO_2 stabilization experiment with land-ice melting. Clim Dyn 29:521–534

Swingedouw D, Braconnot P, Delecluse P, Guilyardi E, Marti O (2007b) The impact of global freshwater forcing on the thermohaline circulation: adjustment of North Atlantic convection sites in a CGCM. Clim Dyn 28:291–305

Vellinga M, Wood RA (2002) Global climatic impacts of a collapse of the atlantic thermohaline circulation. Clim Change 54:251–267

Vettoretti G, Peltier WR (2003) Post-Eemian glacial inception. Part II: elements of a cryospheric moisture pump. J Clim 16:912–927

Wood RA, Keen AB, Mitchell JFB, Gregory JM (1999) Changing spatial structure of the thermohaline circulation in response to atmospheric CO_2 forcing in a climate model. Nature 399:572–575

Yoshimori M, Reader MC, Weaver AJ, McFarlane NA (2002) On the causes of glacial inception 115 kaBP. Clim Dyn 18:383–402

Zheng W, Braconnot P, Guilyardi E, Merkel U, Yu Y (2008) ENSO at 6ka and 21ka from ocean-atmosphere coupled model simulations. Clim Dyn 30(7–8):745–762